Mechanically and thermally stable, transparent electrodes with silver nanowires encapsulated by atomic layer deposited aluminium oxide for organic optoelectronic devices

Shuanglong Wang, Shiwei Wu, Zhitian Ling, Huimin Chen, Hong Lian, Xavier Portier, Fabrice Gourbilleau, Tomasz Marszalek, Furong Zhu, Bin Wei, et al.

Mechanically and thermally stable, transparent electrodes with silver nanowires encapsulated by atomic layer deposited aluminium oxide for organic optoelectronic devices

Shuanglong Wang [a,b,1], Shiwei Wu [a,1], Zhitian Ling [a], Huimin Chen [a], Hong Lian [a], Xavier Portier [c], Fabrice Gourbilleau [c], Tomasz Marszalek [b], Furong Zhu [d], Bin Wei [a], Tao Xu [a,*]

[a] School of Mechatronic Engineering and Automation, Key Laboratory of Advanced Display and System Applications, Ministry of Education, Shanghai University, 200072, Shanghai, China
[b] Max Planck Institute for Polymer Research, Ackermannweg 10, 55128, Mainz, Germany
[c] CIMAP, Normandie Univ, ENSICAEN, UNICAEN, CEA, CNRS, 6 Boulevard Maréchal Juin, 14050, Caen Cedex 4, France
[d] Department of Physics, Research Centre of Excellence for Organic Electronics and Institute of Advanced Materials, Hong Kong Baptist University, Kowloon Tong, Hong Kong, China

Keywords:
Silver nanowires
Atomic layer deposition
Nonfullerene organic solar cells
Polymer light-emitting diodes
Flexible
Stability

A B S T R A C T

Flexible conductive electrodes are essential components for organic optoelectronic devices (OODs). One of the main challenges in the development of flexible OODs is to achieve an optimal combination of photoelectrical properties, enhanced flexibility and stability in transparent conductive electrodes (TCEs). In this work, high-performance flexible nonfullerene organic solar cells (OSCs) and polymer light-emitting diodes (PLEDs) based on TCEs of silver nanowires (AgNWs) encapsulated with an ultra-thin atomic layer deposited aluminum oxide (Al_2O_3) have been demonstrated. The hybrid AgNWs/Al_2O_3 composite electrodes with enhanced thermal, ambient and mechanical stabilities enable an efficient flexible transparent electrode with high transmittance and conductivity, which can synergistically optimize the device performance of nonfullerene OSCs and PLEDs. The maximum power conversion efficiency value of 7.03%, as well as a current efficiency of 7.26 cd A^{-1} for flexible OSCs and PLEDs are achieved, respectively. Notably, excellent flexibility, long-term atmospheric and thermal stabilities have been systematically investigated and demonstrated. These results provide a new design platform for the fabrication of high-performance, flexible transparent electrodes, which can be further explored in a wide range of organic optoelectronics field.

1. Introduction

New-generation organic optoelectronic devices (OODs) such as organic solar cells (OSCs) and polymer light-emitting devices (PLEDs) have appealed great interest and are promising candidates in solid-state lighting and renewable energy applications due to their distinct advantages of large-scale solution processing, cost-effective and flexibility [1–4]. High-performance foldable and transformable conductive electrodes are a critical component for flexible OSCs and PLEDs, which need to be optimized by high transmittance in the visible-light region, excellent electrical conductivity and mechanical stability [5,6]. Currently, the most commercially used transparent electrode in OODs is indium-tin-oxide (ITO). However, its role in flexible and wearable electronics is limited because of its inherent drawbacks of rigidity, brittleness, the scarcity of indium, as well as high-temperature and high-vacuum deposition processing technique [7,8]. Consequently, these shortcomings of ITO incite the development of novel flexible transparent electrodes (FTEs) for new generation optoelectronics. Nowadays, alternative materials for FTEs have been developed to replace ITO including graphene, carbon nanotubes, polymers, metal grids and metallic nanowires [9–13]. Among these materials, silver nanowires (AgNWs) are an appealing candidate because of the appropriate opto-electrical properties, large area and roll-to-roll processing [14–16]. Recently, a high-performance top-illuminated all-solution-processed flexible OSC, comprising of a polymer/AgNWs-based transparent top anode has been demonstrated

[17].

Despite significant advantages over competitors to replace ITO, several problems should be solved for AgNWs-based FTEs [18]. Firstly, during the solution depositing process, the randomly distributed nanowires could become protuberant, resulting in large surface roughness. Secondly, due to the nanoscale size effect, AgNWs tend to melt at a significantly lower temperature (~200 °C) comparing with the bulk silver. Furthermore, the electrical properties of AgNWs may become instable due to long-lasting Joule heating at the junctions between AgNWs [19]. Thirdly, the AgNWs suffer rapid oxidation when exposed to humid air. So the chemical stability of the electrode in organic electronic devices requires amelioration. When the AgNWs worked as a transparent electrode in OODs on which the poly(3,4-ethylenedioxythiophene):poly(styrenesulfonate) (PEDOT:PSS) solution is subsequently deposited, the acidity of PEDOT:PSS can severely damage the AgNWs electrode [20]. Many strategies have been explored to address the aforementioned shortcomings of AgNWs-based FTEs. For example, it has been reported that the use of neutral-pH PEDOT:PSS as the modification layer can improve chemical stability of AgNWs electrode, but the performance of resulting AgNWs/PEDOT:PSS composite electrode is still limited because of the degradation of PEDOT:PSS at a certain high temperature [21]. A tandem layer of zinc oxide (ZnO)/AgNWs/ZnO was reported to enhance the thermal stability of the AgNWs. However, a large thickness of ZnO film (~33 nm) is needed to ensure the protection of AgNWs using sputtering method, which hinders the widespread use for large-area applications [22]. As a result, it is still necessary to develop an effective encapsulation layer on AgNWs-based electrodes.

An effective method is to use the low-temperature atomic layer deposition (ALD) processing, taking its unique advantage of precise thickness control, excellent conformal and pin-hole free coverage ability [23,24]. Indeed, ALD deposited metal oxide films are usually introduced in commercial silicon based solar cell production, whereas there are few literatures about the OODs using this method [25,26]. Recently, Hwang et al. reported that an ultra-thin layer of ALD processed aluminum oxide (Al_2O_3) film grow perpendicularly on the surface of AgNWs, making a perfect conformal coating around individual nanowire and junction, which can effectively improve thermal, chemical and mechanical stabilities of the AgNWs-based FTEs [27]. It is also reported that use of ALD-ZnO coated AgNWs can be applied in PLEDs as FTEs [28]. However, the device performances have not been optimized and the versatility of this method in diverse OODs needs to be further explored.

In this work, we reported a low temperature processed high-performance flexible FTEs based on AgNWs encapsulated by atomic layer deposited ultra-thin Al_2O_3 films. The resulting composite electrode showed excellent mechanical flexibility, long-term atmospheric and thermal stabilities. The surface morphology and the interface structure of AgNWs/Al_2O_3 composite electrode were systematically analyzed by means of scanning electron microscope (SEM), atomic force microscopy (AFM), high-resolution transmission electron microscopy (TEM) and chemical mapping by energy dispersive X-ray (EDX) spectroscopy. Such FTEs were applied in different flexible OODs, giving a high power conversion efficiency (PCE) of 7.03% in flexible nonfullerene OSCs, as well as a current efficiency (CE) of 7.26 cd A^{-1} in PLEDs. Finally, the flexible devices demonstrated excellent mechanical and storage stability, illustrating promising application potentials of the AgNWs/Al_2O_3 FTEs in a variety of efficient and robust OODs.

2. Experiment section

2.1. Materials

AgNWs solution was ordered from BlueNano Company. The average diameter and length of the AgNWs are about 30–60 nm and 15–30 μm, respectively. Poly(methyl methacrylate) (PMMA), Chlorobenzene and 1,8-diiodooctane were ordered from Sigma Aldrich. PEDOT:PSS was ordered from Heraeus. Nonfullerene active materials poly[(2,6-(4,8-bis(5-(2-ethylhexyl)thiophen-2-yl)-benzo[1,2-b:4,5-b']dithiophene))-alt-(5,5-(1′,3′-di-2-thienyl-5′,7′-bis(2-ethylhexyl)benzo[1′,2′-c:4′,5′-c'] dithiophene-4,8-dione))] (PBDB-T) and 3,9-bis(2-methylene-(3-(1,1-dicyanomethylene)-indanone))-5,5,11,11-tetrakis(4-hexylphenyl)-dithieno[2,3d:2′,3′-d']-*s*-indaceno[1,2-b:5,6-b'] dithiophene) (ITIC) were ordered from Solarmer. Super Yellow PPV (SY-PPV, PYD-132) was purchased from Xi'an Polymer Light Technology Corp. The small-molecular material 8-Hydroxyquinolinolato-lithium (Liq) was purchased from e-Ray Optoelectronics Corp. Polyethylene terephthalate (PET) substrates were purchased from CSG Holding Co. Ltd. All chemicals and regents purchased with commercial sources in this work were used as received unless otherwise stated.

2.2. Fabrication of AgNWs/Al_2O_3 FTEs

The PET substrate was firstly washed by detergent, de-ionized water and ethanol, respectively. PMMA solution (80 mg ml^{-1}) was then spin-coated on PET for 60 s at a speed of 1000 rpm, followed by an annealing at 110 °C for 10 min. Then, AgNWs solution was deposited on the PMMA covered PET slide prior to annealing at 110 °C for 15 min to remove residual solvents. After that, mechanical pressure was loaded by a custom-made compressor controlled by an air pressure boosting device. The substrates were finally transferred into a vacuum chamber of ALD. Al_2O_3 layers with five different thicknesses of 1, 2, 4, 10 and 20 nm were deposited by using ALD technique. The ALD deposition processing was carried out in a TFS200 Beneq and the trimethylaluminum and H_2O were employed as the reactants. The deposition rate of Al_2O_3 was 0.1 nm/cycle and the growth temperature was 110 °C. The thickness of the Al_2O_3 was accurately fixed by controlling the cycle numbers.

2.3. Fabrication of flexible nonfullerene OSCs and PLEDs

The device structure of flexible nonfullerene OSCs was PET/FTEs/PEDOT:PSS/PBDB-T:ITIC/Liq/Al. Here, PEDOT:PSS used as hole injection layer (HIL) was filtered through a 0.45 μm syringe filter and deposited to the FTEs/PET substrate by spin-coating at a speed of 3000 rpm, and then annealed at 110 °C for 30 min. Active layer of PBDB-T:ITIC was then spin-coated at 2000 rpm for 60 s, while the thickness of the active films was about 110 nm. To fabricate the active layer, 10 mg of PBDB-T and 10 mg of ITIC were dissolved in 1 mL of chlorobenzene, mixed with 0.03 mL of 1,8-diiodooctane. Finally, Liq (1 nm) and Al (100 nm) were thermally evaporated onto the active layer in a vacuum evaporation system by using a shadow mask at a base pressure of about 1×10^{-5} mbar. The deposition rates for the organic functional materials and Al electrode were 0.6 and 5.0 Å s^{-1}, respectively.

For the fabrication of flexible PLEDs, the SY-PPV material dissolved in toluene with the concentration of 5 mg mL^{-1} and filtered before the deposition on the PEDOT:PSS HIL at 1000 rpm for 60 s to output an uniform emission layer (EML). Then the EML was thermally annealed at 60 °C for 20 min. PEDOT:PSS HIL and Liq/Al were processed as previously described for the flexible nonfullerene OSCs.

2.4. Characterization

The optical transmittances and sheet resistances (R_s) of the transparent electrodes were measured by using a UV–vis spectrophotometer (HITACHI Ue3900H) and a 4-point probe system (RS8, BEGA Technologies), respectively. All the results are measured at least five times to obtain the average values. The surface morphological images of the AgNWs/Al_2O_3 electrodes were analyzed by using SEM (HITACHI S-4800) and AFM (Nanonavi SPA-400SPM). The TEM samples were prepared by using a Focused Ion Beam (FIB) system (HELIOS Nanolab 600 from FEI). Transmission electron microscopy observations were performed using a double corrected ARM200F cold FEG JEOL microscope operated at 200 kV and equipped with an energy dispersive X-Ray (EDX)

spectrometer (CENTURIO from JEOL). Scanning transmission electron microscopy (STEM) combined with a High Angle Annular Dark field Detector (HAADF) allowed chemical analyses. STEM EDX mapping was also carried out and the chemical maps presented hereafter are 256 x 256 maps, with an acquisition time of 5 msec per pixel and about 1000 counts per seconds. All the digitized images were recorded and analyzed with DIGITAL MICROGRAPH (DM2 version) from GATAN.

The typical current density versus voltage (*J-V*) characteristics of the flexible nonfullerene OSCs were tested with a source meter (Keithley 2400) under illumination of 100 mW cm^{-2} with AM 1.5G simulated solar spectrum. The external quantum efficiency (EQE) spectra of the solar cells were measured on a 7-SCSpec solar cell measurements system. The current density-voltage-luminescence (*J-V-L*) characteristics of PLEDs were tested using a PR-650 Spectra Colorimeter and a Keithley 2400 source meter. The mechanical flexibility of the nonfullerene OSCs and PLEDs was tested using a custom-made bending test machine and the bending radius was 5 mm. All the stability of the resulting device was measured with a simple UV curing epoxy resin encapsulation.

3. Results and discussion

The fabrication process of the AgNWs/Al_2O_3 FTEs is illustrated in Fig. 1a. Briefly, AgNWs were first deposited on the PMMA/PET substrate by spin-coating, then pressed partially into PMMA matrix to reduce the surface roughness. Ultra-thin Al_2O_3 films with various thicknesses were finally deposited onto AgNWs. SEM images of the AgNWs/Al_2O_3 composite films clearly show that the average diameter of the underlying AgNWs network increases with the thickness of the Al_2O_3 encapsulation layer from 0 to 2 nm, giving evidence of the good coverage of Al_2O_3 layer on the surface, as shown in Fig. 1b–d. The SEM images for AgNWs encapsulated with 4, 10, and 20 nm of Al_2O_3 are illustrated in Fig. S1. It is known that smooth morphology and uniform coverage of Al_2O_3 encapsulation layer on AgNWs electrode are important for minimizing the roughness and potential leakage current generated in organic devices. Here, AFM observations were used to further analyze the surface morphologies of the resulting AgNWs/Al_2O_3 FTEs. The AFM images (Fig. 1e–g) of the AgNWs/Al_2O_3 network show larger diameter for AgNWs encapsulated by Al_2O_3 layers, which are consistent with the SEM analysis.

To validate the thermal stability of the electrodes coated with Al_2O_3 layer at high temperature, AgNWs encapsulated by Al_2O_3 layer with various thickness (0, 1 and 2 nm) were annealed at 150, 200, and 250 °C for 30 min in atmosphere. It has been reported that an abrupt decrease in electrical performance can be observed at temperatures above 180 °C [29]. Fig. 2 shows the evolution of the surface morphologies of AgNWs/Al_2O_3 composite films under various thermal conditions. Both pristine and Al_2O_3 coated AgNWs were found to remain intact in networks at 150 °C. However, the coalescence of the nanowires into droplets were observed at 200 °C for pristine AgNWs, as shown in Fig. 2b. After annealing at 250 °C, most of the AgNWs agglomerated into balls and the SEM image showed only discrete Ag nanoparticles (see Fig. 2c). The low magnification image of pristine AgNWs annealed at 250 °C is shown in Fig. S2. It is expected that the thermal stability of AgNWs coated with Al_2O_3 can be greatly enhanced. Al_2O_3 has a relatively high melting temperature close to 2070 °C which greatly exceeds that of silver. Even nanoscale alumina film can withstand high annealing

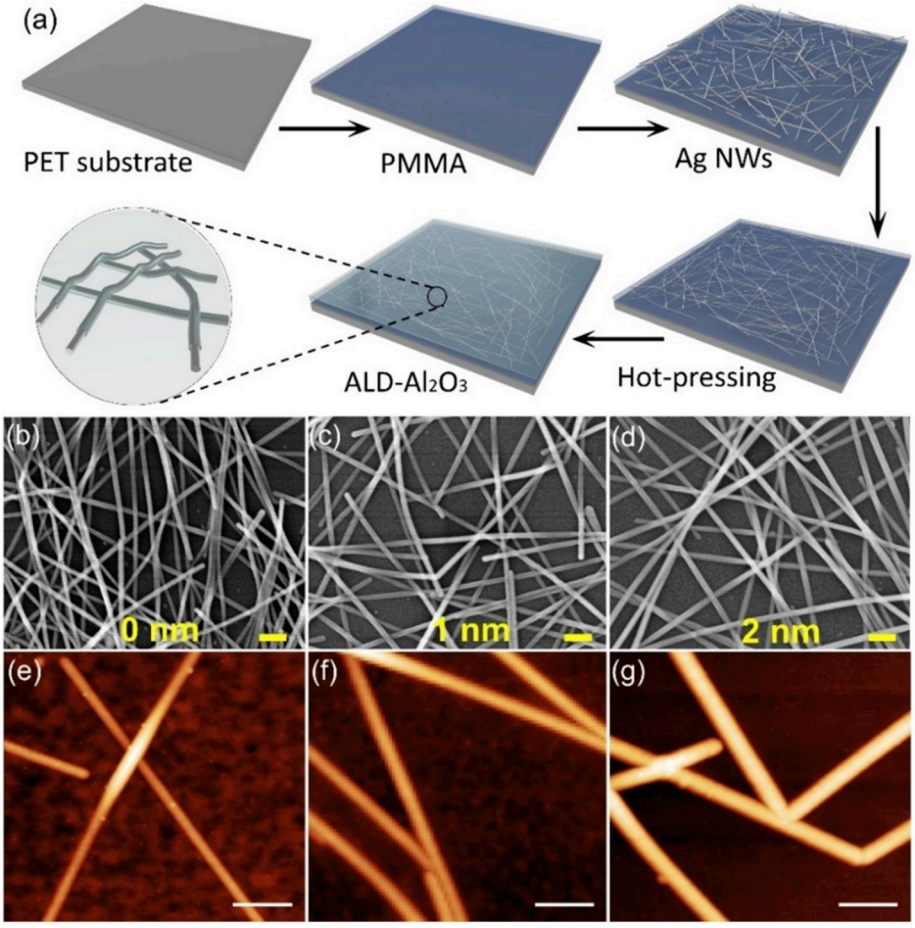

Fig. 1. (a) Schematic representation of the fabrication of the AgNWs/Al_2O_3 composite films. SEM images of (b) pristine AgNWs and AgNWs/Al_2O_3 composite films with various Al_2O_3 thicknesses of (c) 1 nm and (d) 2 nm (The scale bar is 200 nm). (e–g) AFM images of AgNWs/Al_2O_3 composite films corresponding to (b–d). The scale bar is 200 nm.

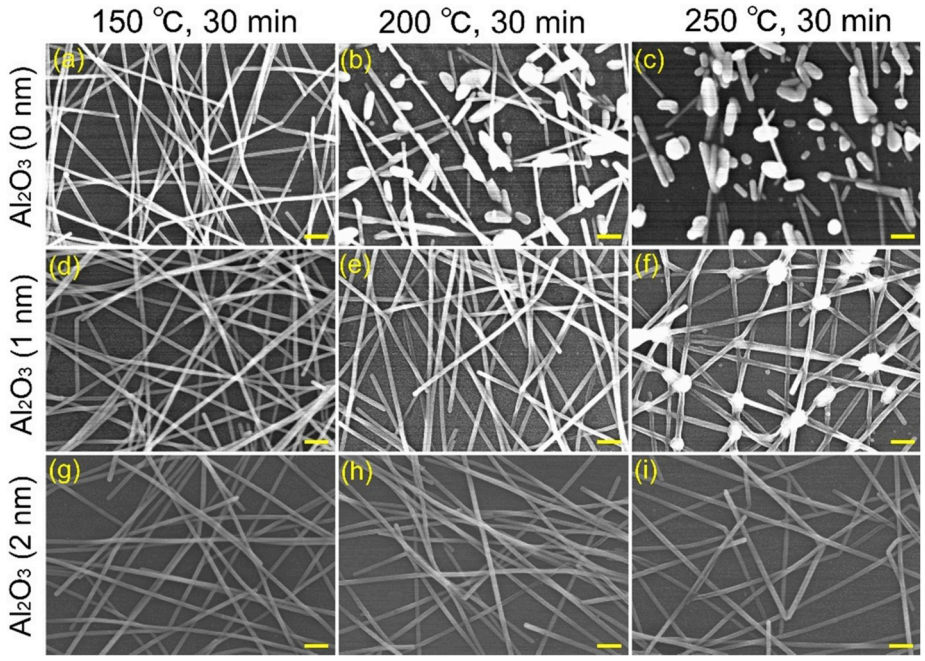

Fig. 2. SEM morphology of AgNWs film with Al_2O_3 films of (a–c) 0 nm, (d–f) 1 nm and (g–i) 2 nm after annealing at different temperatures for 30 min. The scale bar is 200 nm.

temperatures, well over the processing temperatures required for general optoelectronic devices processing [30]. In addition, some works has reported that the trimethyl-aluminum precursor of ALD-Al_2O_3 can adsorb strongly on Ag surface, resulting in the conformal Al_2O_3 encapsulation on the AgNWs [31]. When Al_2O_3 layers were coated onto AgNWs, no samples showed agglomeration on the junctions. For samples heated at 250 °C, the sample with an Al_2O_3 layer thickness of 1 nm shows a few droplets and junction deterioration, as shown in Fig. 2f, which could be attributed to incomplete coverage of the Al_2O_3 coating at low thickness. For comparison, the AgNWs electrode remained the same morphology with no significant coalescence even after annealing at 250 °C with the thickness of Al_2O_3 layer up to 2 nm, as shown in Fig. 2i. Similar thermal stability was observed for AgNWs encapsulated with 4, 10, and 20 nm of Al_2O_3 (Fig. S3). As a result, the conformal Al_2O_3 films with the minimized thickness of 2 nm Al_2O_3 highlights the efficiency of this method that prevents effectively the AgNWs from heating failure at a significantly high temperature (250 °C) for a long duration time. Considering the practical application for optoelectronics fabrication processes involving a post-annealing step for considerable long time, it is expected that the AgNWs/Al_2O_3 electrode can be successfully employed in view of its excellent thermal stability.

To quantitatively analyze the efficacy of the encapsulation layer with

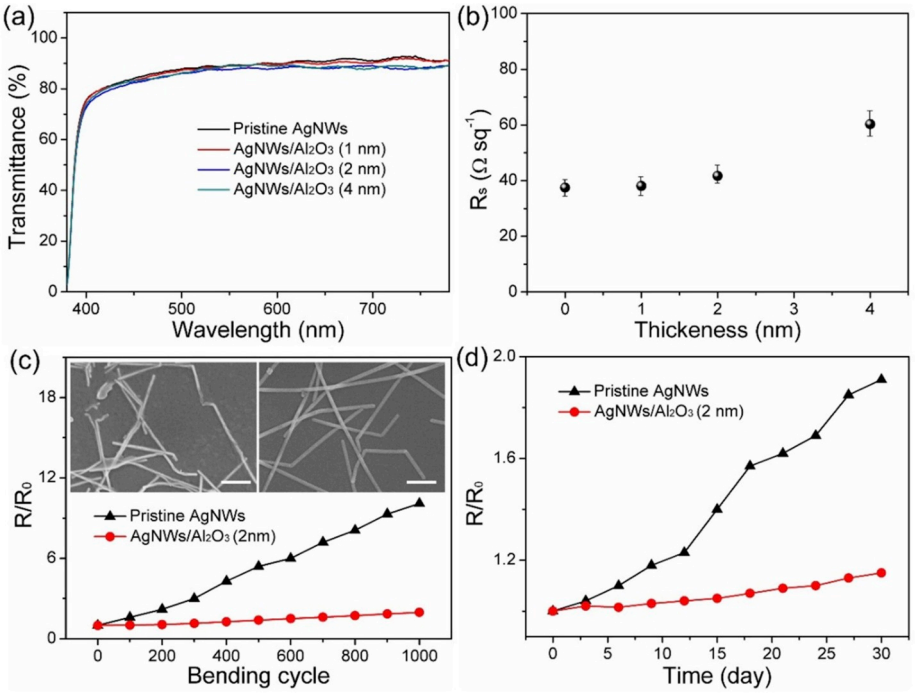

Fig. 3. (a) Transmittance and (b) the corresponding sheet resistance values of AgNWs networks with various thicknesses of Al_2O_3 encapsulation layer. All the samples are prepared on PET substrate. (c) Evolution in R_s versus the number of cycles during the bending test of AgNWs and AgNWs/Al_2O_3. Inset: SEM images of pristine AgNWs film (left photo) and AgNWs/Al_2O_3 composite film (right photo) after the bending tests. The scale bar is 400 nm. (d) Evolution in R_s of pristine AgNWs and AgNWs/Al_2O_3 composite film at a relative humidity of 35% and room temperature condition.

several thicknesses of ALD-Al_2O_3 films, the optical and electrical properties of various AgNWs/Al_2O_3 films were then measured. Fig. 3a shows the results of transmittance for the AgNWs/Al_2O_3. The highest average transmittance value of 86.7% in the visible range was obtained for pristine AgNWs film. The transmittance of the AgNWs/Al_2O_3 (1 nm) composite film was 86.1%, quite close to that of the pristine AgNWs. For comparison, the AgNWs/Al_2O_3 (2 and 4 nm) showed transmittance of 85.3 and 84.4%, respectively. Fig. 3b illustrates the R_s of AgNWs electrodes before and after deposition of 1, 2, and 4 nm Al_2O_3. The addition of an insulating Al_2O_3 film onto AgNWs could certainly increase the R_s, it is thus essential to use an ultra-thin Al_2O_3 film to minimize this negative effect. In our case, the increase of R_s remained small with only 11.3% after depositing 2 nm Al_2O_3 layer. This indicates that the ultra-thin Al_2O_3 coating carried out at the ALD temperature of 110 °C did not significantly alter the electrical properties of the Ag nanowire at a certain low thickness. When the thickness of Al_2O_3 is up to 4 nm, the R_s is dramatically enhanced. As a result, the thickness of Al_2O_3 layer should be optimized to the lowest value for which can still show effective thermal protection. It is important to note that the AgNWs networks with a thicknesses of Al_2O_3 at 2 nm remained intact after high temperature annealing, so the following experiments were performed by using AgNWs electrodes coated with 2 nm of Al_2O_3 to ensure optimal performance.

It is known that good air stability and mechanical durability are critical for the flexible organic optoelectronics [32,33]. Here, we investigated the mechanical durability of the pristine AgNWs and optimized AgNWs/Al_2O_3 (2 nm) electrode by measuring the R_s changes with a bending radius of 5 mm. As shown in Fig. 3c, after 1000 bending cycles, the R_s of AgNWs/Al_2O_3 film increased slightly. In contrast, the R_s increase of pristine AgNWs films rapidly doubled after only 100 bending cycles and increased about 10 times after 1000 bending cycles. These results confirm the excellent mechanical durability of our AgNWs/Al_2O_3 FTEs. SEM observations were performed on pristine AgNWs and AgNW/Al_2O_3 samples after the bending test, as shown in the inset of Fig. 3c. It can be clearly found that part of AgNWs are removed from the substrate after the bending test (see left image), whereas the AgNWs/Al_2O_3 composite film (right) shows a negligible change of morphology and are still well connected (see right image). Such measurements confirm the effect of Al_2O_3 on the flexibility of AgNWs electrode.

The long-term storage stability of the pristine AgNWs and AgNWs/Al_2O_3 composite electrode was also demonstrated. Fig. 3d shows the R_s variations of the AgNWs and AgNWs/Al_2O_3 (2 nm) that were exposed in ambient air and relative humidity of 35%. The R_s of the pristine AgNWs network rapidly increased by 23% in 12 days, while further increase of 91% in resistance was observed for longer exposure up to 30 days. However, the R_s for the AgNWs/Al_2O_3 (2 nm) composite electrode increased slight ~15% after exposure under the same experimental condition for 30 days. The possible reason of the significant increase of R_s in the case of pristine AgNWs has been reported in the literature, which can be mainly attributed to the corrosions by environmental oxygen and sulfur [34,35]. In the case of Al_2O_3, it has been shown to be an excellent barrier material as metal oxide [36]. The good intrinsic corrosion resistance of Al_2O_3 coated around the AgNWs can impede the oxidation of the AgNWs and their junctions, consequently increasing the stability for the AgNWs/Al_2O_3 electrodes.

To evaluate the interface between AgNWs and the ultra-thin Al_2O_3 layer, high-resolution TEM observations were performed on the cross-section of AgNWs/Al_2O_3 composite film. Fig. 4 is a set of TEM images (a) and (b) for the two samples encapsulated by Al_2O_3 layer with thicknesses of 2 and 4 nm. Both images show the cross-section of an AgNW with the electron beam parallel to the revolution axis of the wires. This direction corresponds to the [110] crystallographic direction (according to Miller index) of AgNW. It is interesting to note that the NWs are both divided into several domains with triangular shapes, separated by twin boundaries and a cross point of these boundaries at the middle of the NW. The presence of a 2 nm layer in Fig. 4a with a different grey contrast on the top of the wire suggests that the Al_2O_3 layer covers smoothly the nanowire, giving evidence of the high uniformity and

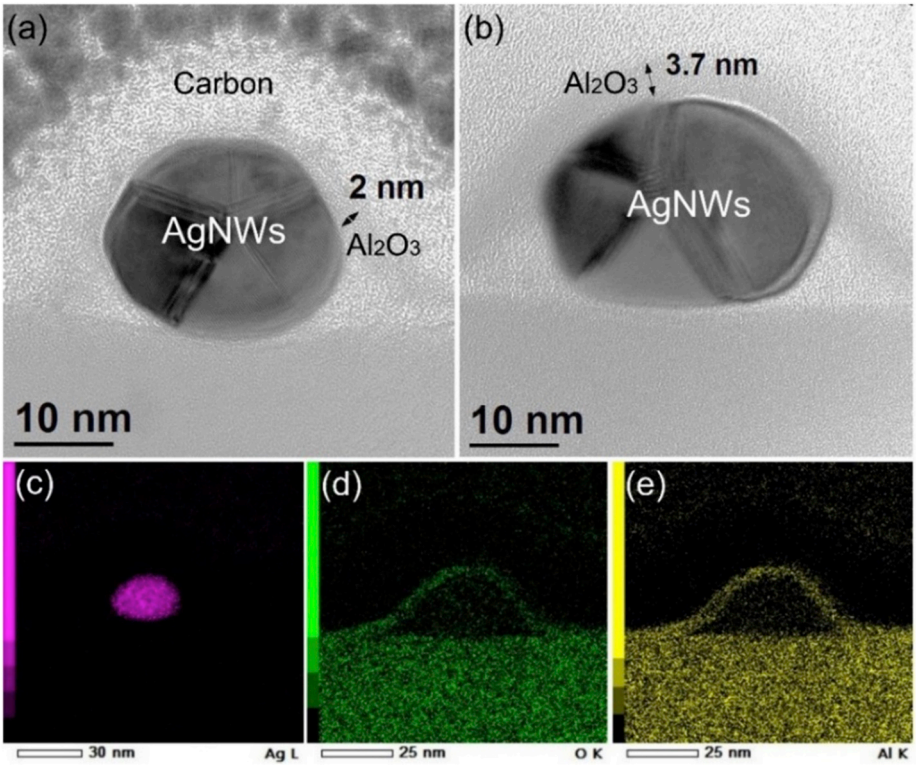

Fig. 4. Cross-sectional TEM image of AgNWs encapsulated by Al_2O_3 layers with thickness of (a) 2 nm and (b) 4 nm. The ALD-Al_2O_3 layer conformally covered the Ag nanowires. (c–e) Energy-dispersive X-ray spectroscopy (EDS) mapping images of the AgNWs/Al_2O_3 composite film.

excellent quality of the ALD deposition. Similar Al_2O_3 layer with a thickness of ~4 nm can be observed in Fig. 4b, indicating the precise control over the thickness at the nanoscale of ALD. Furthermore, chemical analyses were performed to confirm the above statements. Fig. 4c, d and e illustrate STEM EDX mappings for Ag, O and Al, respectively, in the AgNWs/Al_2O_3 composite film. The former one shows undoubtedly the AgNWs and the two latter ones reveal the alumina layer covering the AgNWs, providing a direct evidence of the successful deposition. The EDS analysis confirms that the polymeric residues from the AgNWs ink remained beneath the AgNWs after the coating of the Al_2O_3 layer.

To further demonstrate the viability of the AgNWs/Al_2O_3 composite film as a FTE, nonfullerene OSCs using AgNWs/Al_2O_3 FTE were fabricated with a typical structure, as shown in Fig. 5a. The bulk heterojunction materials consisting of PBDB-T:ITIC blends were employed as the donor and acceptor material to ensure high efficiency of flexible OSCs. Fig. 5b shows the *J-V* characteristics of the resulting OSC devices using AgNWs-based FTEs with or without the optimized (2 nm) Al_2O_3 encapsulation layer. The optimal AgNWs/Al_2O_3-based nonfullerene OSC measured under AM 1.5 G (100 mW cm^{-2}), shows a short-circuit current density (J_{SC}) of 12.35 mA cm^{-2} with an open-circuit voltage (V_{OC}) of 0.89 V and a fill factor (FF) of 63.90%, giving a PCE of 7.03%. The PCE value is lower than the pristine AgNWs based reference sample (7.29%, with $J_{SC} = 12.66$ mA cm^{-2}, $V_{OC} = 0.89$ V, and FF = 64.84%).The slightly inferior PCE of flexible cells using AgNWs/Al_2O_3 anodes is mainly attributed to their lower J_{SC} than that of pristine AgNWs based devices, which is related to the increased sheet resistance induced by the coating of Al_2O_3. The detailed parameters of the devices were summarized in Table 1. The EQE spectra of two different devices are shown in Fig. 5c, the AgNWs/Al_2O_3-based device had a close quantum efficiency comparing with that of the pristine AgNWs-based device in visible light wavelength range. Moreover, it should be mentioned that significantly improved mechanical/thermal/storage stabilities can be further obtained with such novel FTEs, which are essential for the emerging flexible optoelectronics requiring high temperature fabrication processing [37].

To investigate the device mechanical stability, the flexible OSCs are measured for the bending test with different bending times, as shown in Fig. 5d. After finishing 1000 consecutive bending tests with the bending radius of 5 mm, a significant decrease of the device efficiency using pristine AgNWs electrode was observed due to the relatively low mechanical stability of AgNWs. Meanwhile, the flexible OSCs employing AgNWs/Al_2O_3 electrode show considerable good mechanical endurance and can maintain over 90.1% of the original PCE under the same bending test. As a result, the AgNWs/Al_2O_3 based flexible OSCs shows desirable mechanical stability compared to pristine AgNWs based devices.

The thermal stability measurement were also carried out at the

Table 1
Summary of flexible nonfullerene OSC characteristics, averaged from >10 cells.

	V_{oc} [V]	J_{sc} [mA cm^{-2}]	FF [%]	PCE [%]
AgNWs	0.89 ± 0.01	12.66 ± 0.2	64.84 ± 0.3	7.29 ± 0.2
AgNWs/Al_2O_3(2 nm)	0.89 ± 0.01	12.35 ± 0.4	63.90 ± 0.4	7.03 ± 0.2

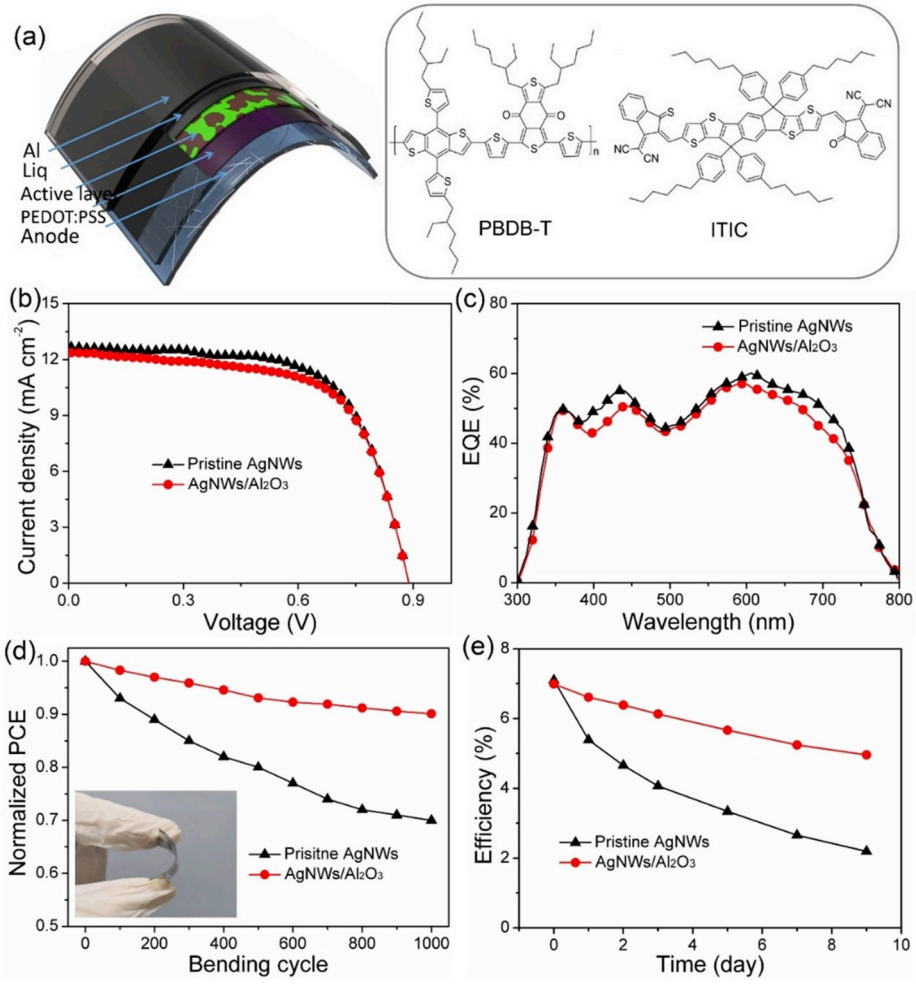

Fig. 5. (a) Device architecture of the nonfullerene OSCs on flexible AgNWs-based PET substrate and chemical structures of the donor and the acceptor used in this study. (b) *J-V* characteristics and (c) the corresponding EQE spectra of the flexible nonfullerene device based on the AgNWs/Al_2O_3 composite electrode as well as the reference cell based on the pristine AgNWs. (d) Normalized PCE of the flexible nonfullerene OSCs after different bending cycles. The inset shows the corresponding device photographs. (e) PCE decays of the resulting flexible encapsulated nonfullerene OSCs as a function of the storage time with various AgNWs based electrodes under ambient conditions.

temperature of 60 °C which is defined as a reference temperature for organic photovoltaic cell in a nitrogen atmosphere in every 10 min [38]. The results are shown in Fig. S4. After the thermal stability test, the efficiency of the devices based on pristine AgNWs decreased from 7.25% to 2.77%, which retained only 38% of its original values. On the contrary, the devices using AgNWs/Al_2O_3 composite electrode demonstrated relatively better thermal stability. The average efficiency of the AgNWs/Al_2O_3 based devices decayed from 7.02% to 3.83%, maintaining 55% of its original value under the same thermal stability test. Since the thermal stability of nonfullerene OSC devices could be very sensitive to active layer morphology factors, the improved thermal stability is likely attributed the composite electrode architecture, which functioned as a heat-insulating scaffold to restrain the reorganization of the active materials when heated [39].

Long-time air stability is also investigated and the result is shown in Fig. 5e, the encapsulated devices based on pristine AgNWs electrode are completely degraded after 9 days, retaining only 30% of the original efficiency, which is mainly caused by the corrosion of AgNWs from the acidic PEDOT:PSS which is employed as HIL. On the contrary, the flexible OSC device using AgNWs/Al_2O_3 composite anode show enhanced environmental stability, resulting in over 71% of the pristine PCE after 9 days. It is worth noting that the moisture can easily access the active layer through the PEDOT:PSS due to its hygroscopicity property [40,41]. However, the Al_2O_3 coating can effectively prevent water eroding the nonfullerene active layer. As a result, the excellent mechanical, thermal and long-term air stabilities of flexible OSCs with a PCE>7% are clearly demonstrated.

Finally, to demonstrate the compatibility of the AgNWs/Al_2O_3 composite electrode in light-emitting devices, we fabricated a flexible PLED using an as-produced AgNWs/Al_2O_3 as anodes onto a PET substrate. The molecular structure of SY-PPV is illustrated in Fig. S5. The device architecture is illustrated in Fig. 6a. Fig. 6b and c shows the corresponding characteristics of resulting PLED devices. Both devices with pristine AgNWs and AgNWs/Al_2O_3 composite anodes showed low leakage currents with a turn on voltage of 3.2 and 3.4 V due to the high conductivity of AgNWs. The measured maximum luminance were 14500.0 and 13576.4 cd m^{-2} for the two flexible PLEDs, while the maximum CE values of 8.47 and 7.26 cd A^{-1} were achieved (see Table 2). The corresponding Commission Internationale de L'Eclairage (CIE) coordinates was located at (0.41, 0.56) (Fig. S6). More importantly, the device employing AgNWs/Al_2O_3 as composite electrode exhibited good mechanical stability, remaining 79% of the initial brightness of 2000 cd m^{-2} after 1000 bending cycles with the same bending radius (5 mm). On the contrary, the pristine AgNWs network maintained merely 58% under the same bending condition. The superior mechanical stability can be explained by the mechanical flexibility of AgNWs/Al_2O_3 composite electrode, as measured previously. Another possible reason for the decrease in brightness can be attributed to the degradation of the functional layers in the devices, such as the evaporated interficial layer or metal electrode, which can be affected by the mechanical deformation [42].

4. Conclusion

In conclusion, we have demonstrated that the AgNWs/Al_2O_3 composite electrodes provide an effective means to improve the stability of both flexible nonfullerene OSCs and PLEDs devices requiring high processing temperatures. The synergy of solution-processed AgNWs and atomic layer deposited Al_2O_3 led to a transparent conductor with excellent optical and electrical properties, superb thermal, mechanical and environmental features, which simultaneously overcomes the shortcomings of AgNWs-based FTEs. Remarkably, high PCEs up to 7.03% in flexible OSCs as well as outstanding EL efficiencies of up to

Table 2
Summary of flexible PLED characteristics.

	V_{on} [V]	L_{max} [cd m^{-2}]	CF [cd A^{-1}]	EL [nm]
AgNWs	3.2	14500	8.47	540
AgNWs/Al_2O_3	3.4	13567	7.26	540

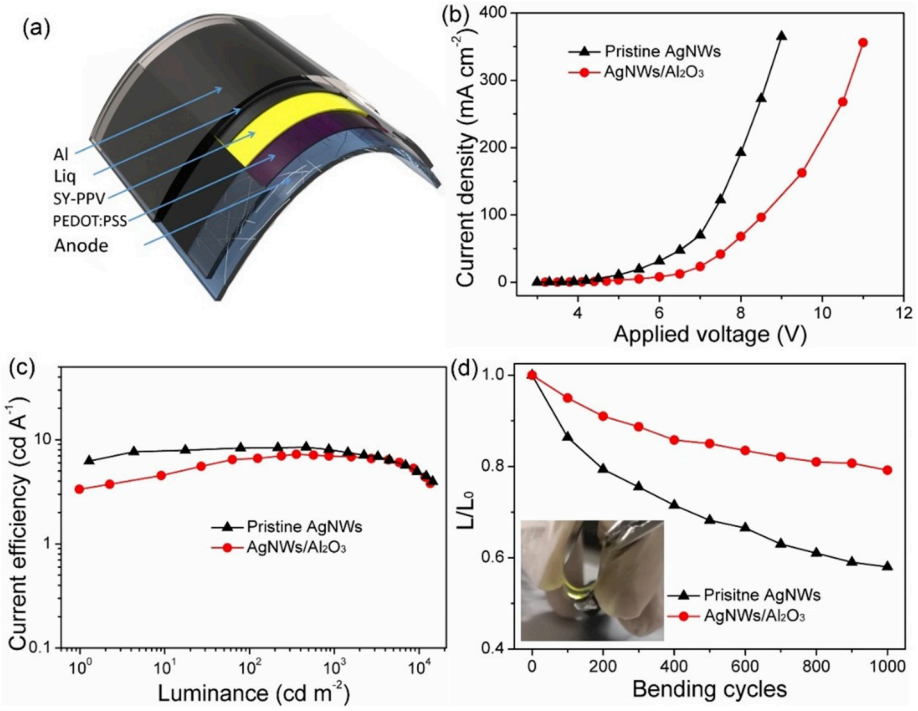

Fig. 6. (a) Schematic illustration of the device architecture for flexible PLED. (b) Current density versus voltage. (c) Current efficiency versus luminance. (d) Normalized luminance of the resulting flexible PLEDs after different bending cycles at a bending radius of 5 mm. The inset shows the corresponding device photographs.

7.26 cd A^{-1} in super yellow based PLEDs built on the AgNWs/Al_2O_3 electrodes were achieved. Finally, the flexible devices demonstrated excellent mechanical and storage stability. We thus believe that this work demonstrates a multifunctional platform, which could provide great potential in a wide variety of optoelectronic applications.

Author contributions

T.X. conceived the idea. S.L.W. and S.W.W. designed the experiments, performed the device fabrication and corresponding data analysis. Z.L., H.C. and H.L assisted with the device characterization and data analysis. X.P., and F.G. conducted AFM and TEM measurements. S. L.W., and T.X. wrote the manuscript. F.Z., and M.T. provided helpful discussions during the project. B.W. and T.X. supervised the project. All authors contributed to the data analysis, discussed the results, and commented on the manuscript.

Declaration of competing interest

The authors declare that they have no known competing financial interests or personal relationships that could have appeared to influence the work reported in this paper.

Acknowledgements

This work was supported by Natural Scientific Foundation of Shanghai (19ZR1419500), Science and Technology Commission of Shanghai Municipality Program (19DZ2281000) and the National Natural Science Foundation of China (61775130, 11974236). X. Portier is grateful to the “Agence Nationale de la Recherche” (ANR) for the EQUIPEX “GENESIS” grant “ANR-11-EQPX-0020” in the frame of the “Investissements d’avenir”. He also wants to thank the “Fond Europeen de Développement Régional” (FEDER) and the Normandie Region. S.L. Wang thanks the China Scholarship Council (CSC) for financial support.

References

[1] Y. Woo, W. Hong, S.Y. Yang, H.J. Kim, J.H. Cha, J.E. Lee, S.Y. Choi, Adv. Electron. Mater. 4 (2018) 1800251.
[2] Y. Miao, K. Wang, B. Zhao, L. Gao, P. Tao, X. Liu, F. Zhu, Nanophotonics 7 (2018) 295–304.
[3] S. Wang, M. Qiao, Z. Ye, D. Dou, M. Chen, Y. Peng, C. Li, iScience 9 (2018) 532–541.
[4] H.W. Bae, S.K. Kim, S. Lee, M.G. Song, R. Lampande, J.H. Kwon, Adv. Electron. Mater. (2019) 1900620.
[5] L. Tang, S. Cheng, L. Zhang, H. Mi, L. Mou, S. Yang, X. Jiang, iScience 4 (2018) 302–311.
[6] S. Jiang, P.X. Hou, M.L. Chen, B.W. Wang, D.M. Sun, D.M. Tang, K.P. Tai, Sci. Adv. 4 (2018) 9264.
[7] S.R. Shin, H.B. Lee, W.Y. Jin, K.J. Ko, S. Park, S. Yoo, J.W. Kang, J. Mater. Chem. C. 6 (2018) 5444–5452.
[8] S. Choi, S.J. Kim, C. Fuentes-Hernandez, B. Kippelen, Opt. Express 19 (2011) 793–803.
[9] T.H. Han, Y. Lee, M.R. Choi, S.H. Woo, S.H. Bae, B.H. Hong, T.W. Lee, Nat. Photonics 6 (2012) 105.
[10] D. Zhang, K. Ryu, X. Liu, E. Polikarpov, J. Ly, M.E. Tompson, C. Zhou, Nano Lett. 6 (2006) 1880–1886.
[11] M.S. White, M. Kaltenbrunner, E.D. Głowacki, K. Gutnichenko, G. Kettlgruber, I. Graz, Z. Major, Nat. Photonics 7 (2013) 811.
[12] G. Jeong, S. Jung, Y. Choi, J. Lee, J. Seo, D.S. Kim, H. Park, J. Mater. Chem. 6 (2018) 24805–24813.
[13] J.H. Kim, J.W. Park, ACS Appl. Mater. Interfaces 10 (2018) 9704–9717.
[14] W. Gaynor, S. Hofmann, M.G. Christoforo, C. Sachse, S. Mehra, A. Salleo, P. Peumans, Adv. Mater. 25 (2013) 4006–4013.
[15] J. Liang, L. Li, K. Tong, Z. Ren, W. Hu, X. Niu, Q. Pei, ACS Nano 8 (2014) 1590–1600.
[16] S. HwanáKo, Nanoscale 9 (2017) 1978–1985.
[17] S. Wang, Y. Zhao, H. Lian, C. Peng, X. Yang, Y. Gao, T. Xu, Nanophotonics 8 (2019) 297–306.
[18] C. Yang, H. Gu, W. Lin, M.M. Yuen, C.P. Wong, M. Xiong, B. Gao, Adv. Mater. 23 (2011) 3052–3056.
[19] T.B. Song, Y. Chen, C.H. Chung, Y. Yang, B. Bob, H.S. Duan, Y. Yang, ACS Nano 8 (2014) 2804–2811.
[20] Y.S. Kim, E.J. Lee, J.T. Lee, D.K. Hwang, W.K. Choi, J.Y. Kim, RSC Adv. 6 (2016) 64428–64433.
[21] S. Chen, L. Song, Z. Tao, X. Shao, Y. Huang, Q. Cui, X. Guo, Org. Electron. 15 (2014) 3654–3659.
[22] A. Kim, Y. Won, K. Woo, C.H. Kim, J. Moon, ACS Nano 7 (2013) 1081–1091.
[23] P. Poodt, R. Knaapen, A. Illiberi, F. Roozeboom, A. van Asten, J. Vac. Sci. Technol. A: Vac., Surf., Film. 30 (2012) 142.
[24] O. Ibrahim Elmi, O. Cristini-Robbe, M.Y. Chen, B. Wei, R. Bernard, D. Yarekha, E. Okada, S. Ouendi, X. Portier, F. Gourbilleau, T. Xu, D. Stiévenard, Nanotechnology 29 (2018) 285403.
[25] W.C. Wang, M.C. Tsai, J. Yang, C. Hsu, M.J. Chen, ACS Appl. Mater. Interfaces 7 (2015) 10228–10237.
[26] B. Wei, Z.Y. Tang, S.L. Wang, C.P. Qin, C.Y. Li, X.W. Ding, Y. Gao, X. Portier, F. Gourbilleau, D. Stiévenard, T. Xu, Nanotechnology 29 (2018) 395204.
[27] B. Hwang, Y. An, H. Lee, E. Lee, S. Becker, Y.H. Kim, H. Kim, Sci. Rep. 7 (2017) 41336.
[28] D. Chen, J. Liang, C. Liu, G. Saldanha, F. Zhao, K. Tong, Q. Pei, Adv. Funct. Mater. 25 (48) (2015) 7512–7520.
[29] H.G. Im, J. Jin, J.H. Ko, J. Lee, J.Y. Lee, B.S. Bae, Nanoscale 6 (2) (2014) 711–715.
[30] G. Guisbiers, S. Pereira, Nanotechnology 18 (43) (2007) 435710.
[31] S.D. Standridge, G.C. Schat, J.T. Hupp, Langmuir 25 (5) (2009) 2596–2600.
[32] X.Y. Zeng, Q.K. Zhang, R.M. Yu, C.Z. Lu, Adv. Mater. 22 (40) (2010) 4484–4488.
[33] B. Hwang, H.A.S. Shin, T. Kim, Y.C. Joo, S.M. Han, Small 10 (16) (2014) 3397–3404.
[34] E. Langereis, M. Creatore, S.B.S. Heil, Van De, M.C.M. Sanden, W.M.M. Kessels, Appl. Phys. Lett. 89 (8) (2006), 081915.
[35] Y. Ahn, Y. Jeong, Y. Lee, ACS Appl. Mater. Interfaces 4 (12) (2012) 6410–6414.
[36] U.S. Lee, J.S. Choi, B.S. Yang, S. Oh, Y.J. Kim, M.S. Oh, H.J. Kim, ECS. Solid. State. Lett. 2 (6) (2013) R13–R15.
[37] L. Li, J. Liang, S.Y. Chou, X. Zhu, X. Niu, Q. Pei, Sci. Rep-UK. 4 (2014) 4307.
[38] L. Derue, O. Dautel, A. Tournebize, M. Drees, H. Pan, S. Berthumeyrie, A. Rivaton, Adv. Mater. 26 (2014) 5831–5838.
[39] R. Wang, S.Y. Chang, L. Meng, W. Huang, J.W. Lee, H.W. Cheng, C. Zhu, Matter 1 (2) (2019) 402–411.
[40] S. Shao, J. Liu, J. Bergqvist, S. Shi, C. Veit, U. Wuerfel, F. Zhang, Adv. Energy. Mater. 3 (3) (2013) 349–355.
[41] H. Zhou, Y. Wang, J. Zhang, Z. Yu, Y. Li, L. Tan, Y. Chen, J. Mater. Chem. C. 6 (2) (2018) 312–319.
[42] S. Wang, J. Yang, T. Xu, D. Dou, Z. Tang, Z. Gao, R. Bachelot, Org. Electron. 64 (2019) 146–153.